International Journal on Smart Material and Mechatronics
IJSMM Vol. 13 No. 2 2026 DOI. 10.20342/IJSMM.13.2. 461
p-ISSN: 2356-5314
e-ISSN: 2460-075X

Characteristics of Friction Surfacing Deposit and its Potential Application for Aluminum Spot Lap Joint

Hasan, Lukmanul Hakim Arma*, Hairul Arsyad, Rudi, Gaffar, Indra
Departement of Mechanical Engineering, Faculty of Engineering
University Hasanuddin, Indonesia
hasan22d@student.unhas.ac.id, armalh@unhas.ac.id, arsyadhairul@eng.unhas.ac.id,
rudi.amme@unhas.ac.id, gaffaralqadri18498@gmail.com, indrarvt@gmail.com
*Corresponding Author

***Abstract*—Friction surfacing is a solid-state surface modification technique capable of producing aluminum deposits with robust metallurgical bonding while reducing thermal degradation of the substrate compared to fusion-based coating methods. Nonetheless, the combined influence of consumable rod diameter and substrate surface roughness on layer formation, mechanical performance, thermal behavior, and potential application as mechanical joints remains inadequately understood. This study examines the effects of rod diameter and substrate surface roughness on aluminum layers produced by friction surfacing and assesses their suitability for aluminum spot-joint applications. AA6061 aluminum alloy served as the consumable rod, while AA1100 was utilized as the substrate. The process was executed at a rotational speed of 3300 rpm and a translational speed of 9 mm/min, with variations in rod diameter and axial load. Characterization involved measurements of bending strength, microhardness, and surface roughness. The results indicated that a 12 mm rod diameter combined with a 25 kg load yielded the highest bending strength of 203.48 MPa, attributed to stable material flow and balanced heat distribution. A lower substrate surface roughness (Ra = 1.070 µm) enhanced bending strength and hardness and facilitated a more uniform thermal distribution during deposition. Conversely, higher surface roughness accelerated heat generation and induced local stress concentrations, thereby diminishing the mechanical performance of the layer. These findings elucidate the relationship between process parameters, surface conditions, and mechanical properties in friction surfacing, demonstrating its potential for aluminum spot-joint formation through deposit formation and flash-based mechanical interlocking mechanisms.**

Friction surfacing; Surface roughness; Bending strength; Aluminum deposit; Aluminum lap joint

I. Introduction

Aluminum is one of the most widely used non-ferrous metals in various industrial sectors [1]. Its physical, chemical, and mechanical properties confer corrosion resistance, and its potential for enhancement through heat treatment renders aluminum strategic for applications in the automotive, aerospace, marine, construction, and electronics industries [2][3]. However, aluminum alloys encounter challenges in fusion welding methods. The primary issue is the presence of a stable, hard Al_2O_3 oxide layer, which has a higher melting point (2050°C) than pure aluminum (660°C). This layer impedes the formation of robust metallurgical bonds and increases porosity, hot cracking, and dimensional instability during welding [4][5]. Consequently, solid-state processes such as friction surfacing (FS) have been developed. In FS, a rotating rod is pressed against a substrate, generating frictional heat and plastic deformation without complete melting [4][6]. The viscoplastic material at the rod tip is deposited as a layer bonded to the substrate. Compared to thermal spraying, plasma spraying, and laser cladding, FS provides strong metallurgical bonding, porosity-free layers, and reduced thermal distortion [7][8]. Numerous studies have demonstrated that FS is an effective solid-state deposition technique for integrating metal materials with distinct characteristics. In this process, the deposit-substrate bond is established through intensive plastic deformation, interatomic diffusion, and mechanical interlocking at the interface. Research by [9] successfully deposited AA6082 aluminum alloy onto an AISI 316 stainless steel substrate using FS, resulting in a defect-free layer with a stable interfacial bond. The study also highlighted the importance of substrate surface topography, which enhances plastic deformation in the contact area and improves bond quality. These findings suggest that substrate surface characteristics are a crucial factor influencing FS effectiveness. Research has shown that bonding in FS is affected by material combinations and thermal conditions during deposition. Depositing aluminum alloys AA6082 and AA7050 onto a Ti6Al4V substrate results in distinct interfacial bonding characteristics. In the AA6082–Ti6Al4V system, higher temperatures promote a thin intermetallic layer, aiding diffusion bonds [10]. Conversely, in the AA7050–Ti6Al4V system, mechanical interlocking plays a greater role between deposit and substrate during FS. This difference underscores the impact of process parameters and material properties on bond quality. Studies have emphasized how process parameters affect deposit morphology and microstructure evolution during deposition. Depositing AA2024-T351 onto an AA7475-T761 substrate by FS produces deposits with stable metallurgical bonding and no macroscopic defects. Axial force and deposition speed were identified as key factors affecting layer morphology and deposit interface quality [11][12]. Similarly, multi-layer FS enables additive structures from different aluminum alloys, including AA5083 and AA2024. Here, dynamic recrystallization during deposition refines grain size in the deposit microstructure, improving interlayer bonding stability [13][14]. A knurled mild steel substrate and a B4C-reinforced AA6082-T6 consumable rod produced a defect-free cladding layer with uniform particle distribution, a stable coefficient of friction, and weight loss of only 1.3 mg under dry sliding wear testing at a load of 10 N [15]. Beyond microstructural considerations, research has examined the impact of material modifications on the mechanical properties of resultant deposits. Depositing AA6061 onto an AA5083 substrate, reinforced with stainless steel 316 particles, led to an approximately 18% increase in coating strength compared to deposits without reinforcing particles, and improved interfacial bonding [16]In the multilayer deposition of aluminum alloys via friction surfacing, interlayer regions demonstrate finer grains and greater recrystallization than the central part of the deposit [13], resulting in increased hardness at interface regions. Layer formation during friction surfacing is influenced by material flow at the rod tip, where intense plastic deformation tends to form the upper part of the deposit with a finer grain size [10][17]. This method is cost-effective and environmentally sustainable for producing uniform metal layers [18]. The quality of friction surfacing (FS) coatings is influenced by process parameters, including axial force, rotational speed, and travel speed [19], [20], [21]. Pin tool configuration, tool tilt angle, and feed rate affect heat distribution, plastic deformation rate, and the bonding mechanism [11], [22], [23]. High rotational speeds can enhance material flow by increasing interface temperatures but may cause defects if excessive flash is produced [24]. Similarly, travel speed affects layer thickness and quality; low speeds risk heat accumulation, whereas high speeds compromise bond strength [25-27] . Additional factors, such as the initial rod condition, heat treatment, and substrate characteristics, contribute to the microstructure and mechanical properties of the deposit [28]. Thermal and microstructural phenomena during the FS process are crucial for coating quality, as temperature distribution is associated with rod geometry and operating parameters [11], [29]. Multilayer FS alters microstructure, influencing grain texture and mechanical properties of aluminum coatings on substrates [30]. While numerous studies have highlighted the effects of process parameters, thermal characteristics, and microstructural evolution in friction surfacing (FS), the application of FS deposits for metal joining, particularly in lap joint configurations, remains underexplored. Most research focuses on coatings and component repair, with a systematic investigation of FS deposits as an alternative joining mechanism lacking. Consequently, this study analyzes aluminum deposits produced via the FS process and assesses their potential as a joining method. It emphasizes axial load and substrate surface roughness, critical factors affecting contact area, heat distribution, material plastic deformation, and interfacial bond quality during FS. Preliminary studies suggest that variations in substrate topography can enhance bond quality through mechanical interlocking and intermetallic diffusion, creating opportunities for advancing friction surfacing-based joining techniques.

II. Material and Methods

Aluminum alloy AA1100 is utilized as both the consumable rod (CR) and the substrate. The hardness values for AA6061-0 and AA1100 are 55 HV and 29 HV, respectively. The chemical composition is provided in Table I. The CR measures 110 mm in length and is available in diameters of 12 mm, 15 mm, and 17 mm. The substrate is a plate with dimensions of 200 mm × 40 mm × 3 mm. The friction surfacing (FS) process employs a modified LC-40A drilling-milling machine, which incorporates a travel speed mechanism and axial loading, as depicted in Fig.1.

TABLE I. Chemical composition AA1100 and AA6061-0 (%wt).

Materials	***AA1100***	***AA 6061-O***
Mg	-	0.975
Si	0.600	0.755
Cu	0.060	0.242
Fe	0.660	0.3073
Zn	-	0.016
Ti	-	0.0262
Mn	-	0.070
Cr	-	0.183
S	0.060	-
Others	Max 0.5	Max 0.5
Al.	Al.	Bal.

Fig. 1. Modified drilling-milling machine for the friction surfacing process

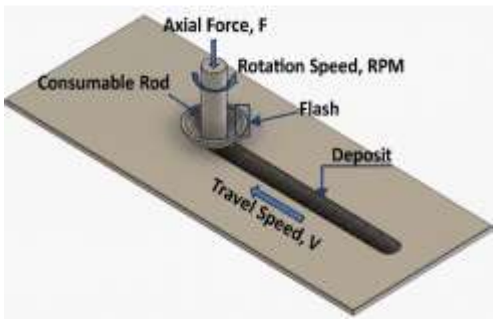

Fig. 2. schematic of the friction surfacing process.

p-ISSN: 2356-5314
e-ISSN: 2460-075X

The friction surfacing process commences with the rotation of the consumable rod (CS) at a speed of 3300 revolutions per minute (rpm), accompanied by the application of axial force until contact with the substrate surface is achieved, thereby generating friction and heat. The CS maintains contact with the substrate until its tip reaches approximately 150 °C. Subsequently, the substrate is moved laterally at a rate of 9 millimeters per minute to form a layer, as illustrated in Fig. 2. To examine the characteristics of the deposit, friction surfacing is performed with axial loads of 15 kg, 20 kg, and 25 kg, in conjunction with surface roughness values of 1.070 µm, 1.261 µm, and 1.491 µm.

Deposit Dimensional Measurement

The characteristics of the deposit were evaluated by measuring its width and thickness following the FS process. These parameters are indicative of the geometry and reflect the axial load and applied pressure across various CR diameters. In lap joint applications, the uniformity of width and thickness is crucial for maintaining integrity and performance, although variations may be observed along the deposited region, as illustrated in Fig. 3.

Fig. 3. Width and thickness of the FS-deposited layers

Bending test

The bending test assesses bending strength, indicating the integrity of the deposit on the substrate. The FS sample is sectioned into specimens by slicing perpendicular to the layer, ensuring the deposit is positioned along the specimen longitudinal axis (Fig. 4). The deposit is smoothed to achieve a flat surface and uniform dimensions. The test uses the three-point bending method (Fig. 5), ensuring bending strength reflects bond strength between deposit and substrate. It is performed using a 5 kN Shimadzu autograph machine at speed of 1 mm/s.

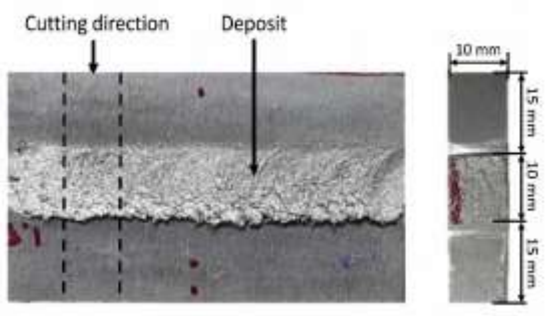

(a) (b)

Fig. 4. (a) Position and direction of FS deposit sampling; (b) dimensions of the bending test specimen.

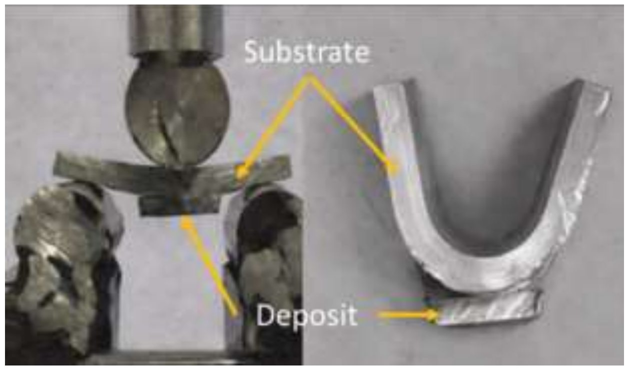

Fig. 5. Bending test and the specimen after testing

Hardness Test

The specimen cross-section is embedded in resin to stabilize it during testing. Hardness testing was performed using the Vickers method with a 0.2 kgf load and 15 seconds indentation dwell time. Indentation locations are shown in Fig. 6.

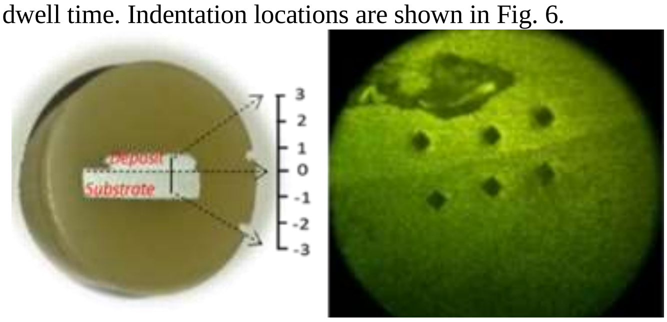

(a) (b)

Fig. 6. (a) Hardness testing point coordinates on the substrate and deposit cross section; (b) three interface hardness testing points (at positions 1 and -1).

Surface Roughness Test

The substrate AA1100 was roughened using abrasive papers #60, #120, and #240, oriented perpendicularly to the deposition direction. Surface roughness (Sa) was quantified according to ISO 25178 using 3D Measuring Laser Microscope, Olympus OLS4100, with a cut-off length of 0.8 mm. Recorded roughness values were 1.491, 1.261, and 1.070 µm, respectively. Roughness profiles are shown in Fig. 7.

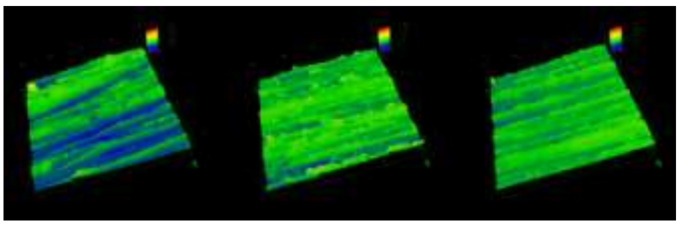

(a) (b) (c)

Fig. 7. Surface profiles, substrate roughness levels: (a) Sa = 1.491 µm; (b) Sa =1.261 µm; (c) Sa= 1.070 µm.

Metallography

Metallography examines the interface condition of substrate and deposit specimens. Specimens are embedded in resin for handling. After progressive grinding and polishing, they are

 p-ISSN: 2356-5314
e-ISSN: 2460-075X

etched using Keller's solution. The interface is then observed with the Olympus OLX400 Optical Measuring Microscope.

III. Result and Discussion

A. Deposit Dimension and Axial Load

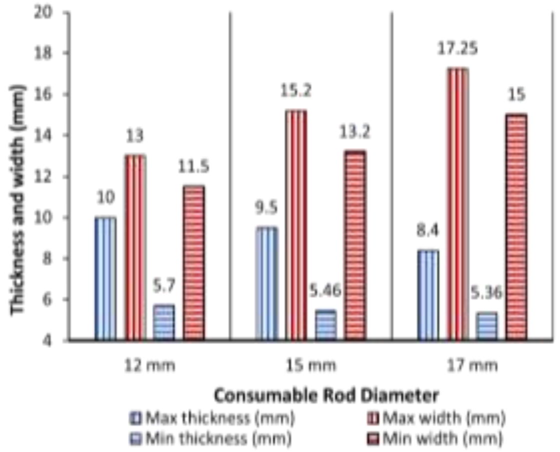

Fig. 8. Correlation between CR diameter and FS coating width and thickness at an axial load 20 kg.

Fig. 8. Illustrates deposit thickness and width as influenced by CR diameter in the FS process under an axial load of 20 kg. This load is transmitted as axial pressure at the CR tip and substrate surface, inducing plastic flow in the CR and forming a layer with width and thickness corresponding to the CR diameter. As indicated in Table II, 12 mm CR produced wider layer, with maximum width difference of 1 mm and minimum of -0.5 mm, whereas other CRs showed smaller differences. This suggests that layer dimensions were affected by the axial pressure exerted by 20 kg load. CRs with larger diameters experienced reduced stress, forming a narrower layer. Axial pressure affected thickness, with the 12 mm diameter CR receiving higher pressure and producing the thickest layer. These observations align with studies linking rod size, rotational speed, and formed-layer width [31][32]. Axial load affects material flow, heat input, and tool penetration depth, thereby influencing the geometry of the welding/deposition [33], [34].

TABLE II. Dimensional of The Deposit Under 20 Kg Axial Load

Diameter CR, D (mm)	Width of deposit, L (mm)		L-D (mm)	
	maximum	*minimum*	*maximum*	*minimum*
12	13	11.5	1	-0.5
15	15.2	13.2	0.2	-1.8
17	17.25	15	0.25	-2

B. Bending Strength, Axial Load and Hardness Vickers.

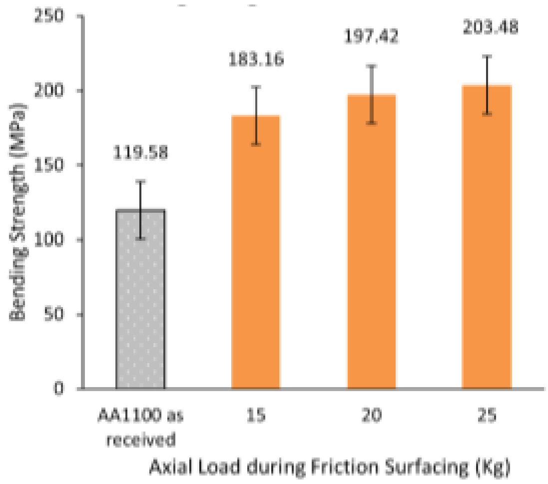

Fig. 9. Bending strength of the substrate+deposit at various FS axial loads using CR=12 mm

The bending force was used to obtain the interfacial shear strength between the substrate and deposit. Fig. 9. Shows that increasing the axial load up to 25 kg increases bending strength. During the FS process, heat and axial load deliver sufficient stress to facilitate metallurgical bonding at the interface, thereby increasing interfacial shear strength. Deposit hardness increases with axial force, which induces material to flow plastically from the tip of the CR to the substrate surface. The bending strength of the substrate plus deposit increased compared to the substrate material alone (AA1100). Increasing axial load during friction surfacing enhances the bending strength of substrate–deposit specimens. Evidence indicates that axial force is the most influential parameter governing hardness and bending performance [35]. Its effect is reflected in coating thickness and width, which contribute to bending improvement, as demonstrated in friction surfacing of Al 6063 onto AISI 316 stainless steel [36].

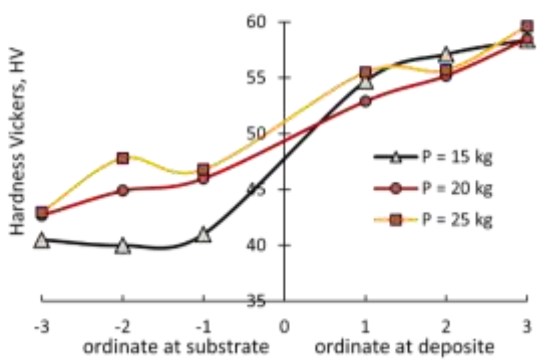

Fig. 10. Hardness profile across the substrate + deposit area at FS axial loads (CR = 12 mm)

Fig. 10. Shows that axial load exerted minimal influence on hardness distribution in the substrate material (AA1100) and deposit material (AA6061-O). Hardness in the deposit area remained nearly uniform across axial loads, with values approximating the hardness of the CR (AA6061-O). The decreased substrate hardness at an axial load of 15 kg may be caused by constant CR rotation under lighter pressure, making heat flow into the substrate more dominant and generating a viscoplastic state at the CR tip from deposits. Heat input into

the substrate can cause grain growth and reduced hardness. A relatively high heat input results in an extended thermal cycle in the heat-affected zone (HAZ), promoting coarser grains that can reduce hardness [37]. Excessive heating with slow cooling during the process can also decrease material hardness [38]. Axial force was found to have the greatest influence on hardness and bending strength [11]. Rotational speed and axial force play significant roles in increasing interface hardness [39]. Axial load plays a dominant role in achieving better hardness and maximum displacement, followed by traverse speed and rotational speed [31]. The deposit formed atop the substrate influences bending strength and hardness, which are critical to the strength of metallic joints, and deposits formed through the FS process also increase interfacial bending strength.

C. Surface Roughness (SA) on Substrate, Bending Strenght, and Hardness Test.

After examining deposits influenced by axial load, focus shifted to surface roughness. Introducing roughness to the substrate enhanced shear strain during the initial stages of the Friction Surfacing process. Increased mechanical resistance from asperities necessitates plastic deformation of the rod tip, promoting intensive dynamic recrystallization (DRX) at the interface. This contributes to heightened hardness and stronger mechanical interlocking between deposit and substrate. The relationship between substrate surface roughness (Sa) and the aluminum layer was analyzed using a rod diameter of 12 mm and a load of 20 kg. Surface roughness (Sa) indicates substrate topography and initial condition prior to the FS process. It influences adhesion, heat distribution, and bonding mechanism between the CR material and substrate. To assess its effect, bending strength and hardness tests were conducted on the contact area of the aluminum layer. The relationship between substrate surface roughness (Sa) and the flexural strength of aluminum during the friction surfacing process is shown in Fig. 11.

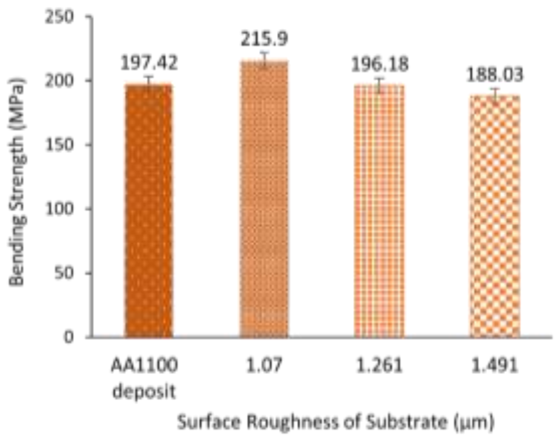

Fig. 11. Bending strength of the aluminium substrate+deposit with varying substrate surface roughness.

As shown in Fig. 11. Surface roughness (Sa) significantly influenced the bending strength of the aluminum layer produced by friction surfacing. At surface roughness 1.070 µm, maximum bending strength reached 215.9 MPa, slightly exceeding AA2024-O. However, increasing surface roughness to 1.491 µm reduced bending strength. These findings suggest that lower (smoother) surface roughness promotes formation of a robust, stable interfacial bond during deposition. Shear strength increases with surface roughness because more asperities act as mechanical interlocks [40]. The decrease in bending strength is attributed to ineffective interlock formation, as the deposit fails to fill deep grooves (high roughness values) on the substrate, leading to void formation. This diminishes metallurgical bonding, mechanical interlocking, and the formation of the effective shear resistance between rod material and substrate, reducing bending strength. In bending tests, interfaces with voids show reduced mechanical interlocking [41]. Increased substrate surface roughness leads to higher push-off strength, reaching up to 45 MPa; the resulting stronger interfacial bond is expected to contribute to enhanced bending behavior in layered materials produced by friction surfacing [42].

Fig. 12. Illustrates the relationship between substrate surface roughness (Sa) and aluminum layer hardness in the friction surfacing process, showing layer's hardness response to initial substrate condition variations.

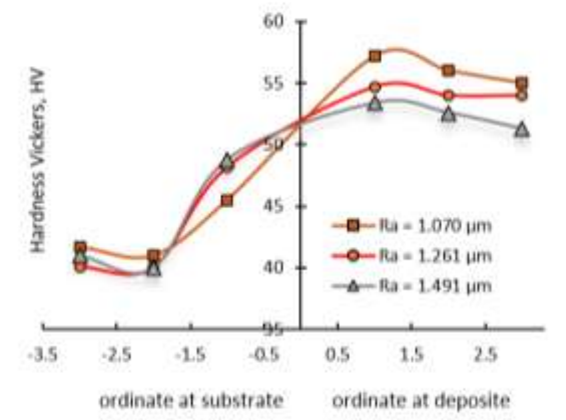

Fig. 12. Hardness and subrate roughness (Sa) for each point.

Fig. 12. presents the hardness test results for two regions: the substrate surface and the aluminium layer produced by friction surfacing. The results show increased hardness at the interface (ordinate −1), indicating the occurrence of dynamic recrystallisation, which generates finer equiaxed grains that impede dislocation motion and increase shear resistance at the bond between the deposit and substrate. These findings demonstrate that substrate surface roughness influences the hardness of the aluminium layer [43]. Substrate roughness has previously been reported to affect frictional Smoother surfaces promote more uniform heat distribution and plastic deformation during deposition, leading to the formation of a harder layer. In contrast, higher roughness induces irregular material flow and local stress concentrations, which reduce hardness through unstable thermal fields and an increased density of defects. Greater roughness also modifies the local mechanical response, causing spatial variations in plastic deformation and contributing to lower and non-uniform hardness intensity and heat generation during friction surfacing [10]. Mechanical analysis also indicates that increasing roughness can create stress-concentration zones that result in higher coating hardness [44]. In addition, roughness alters the

p-ISSN: 2356-5314
e-ISSN: 2460-075X

effective contact area during hardness testing, thereby influencing the measured values [45]. Overall, substrate surface roughness is a key parameter governing the hardness of friction-surfaced layers. As discussed in a review on friction surfacing, the increased hardness in the interface zone arises from dynamic recrystallisation (DRX). This process produces an extremely fine equiaxed grain structure in the TMAZ, which effectively constrains dislocation movement in accordance with the grain boundary strengthening mechanism described by the Hall–Petch relationship.

D. Interface Substrate and Deposite.

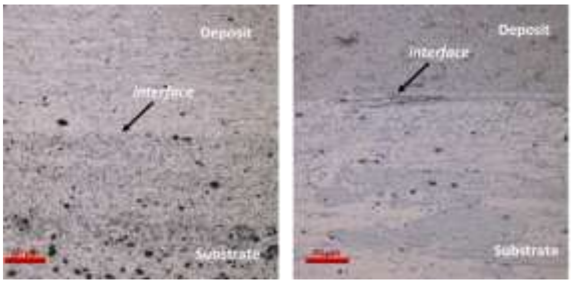

(a) (b)

Fig. 13. Interface between the substrate and deposit: (a) As-received AA1100 substrate and (b) AA1100 Substrate with Sa = 1.070 µm

Fig. 13. illustrates the deposit-substrate interface, where metallic bonding is evident. The substrate microstructure revealed fine grains attributable to dynamic recrystallization. In contrast, the lower section exhibited elongated, flattened grains, indicative of pressure exerted during the FS process

E. Proposed Application: Spot Lap Joint Mechanic.

The friction surfacing process joins metals through metallurgical and mechanical bonds. Metallurgical bonding occurs where pressure, rotation, and heat disrupt oxide layers, enabling interatomic diffusion between similar metals. Experimental findings on the dimensional and mechanical properties of friction surfacing deposits indicate this method's potential for joining two overlapping metal plates. One plate has a joint hole for forming a spot friction deposit that seals the hole and secures both plates through fusion and mechanical means. This technique mitigates machine vibration during extended deposition by eliminating travel speed parameters.

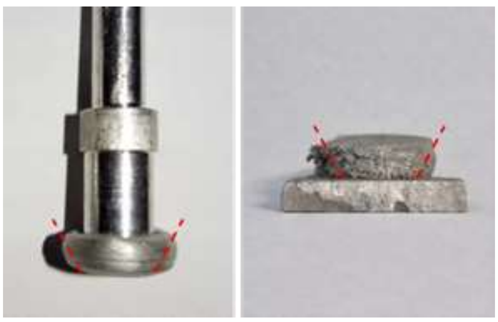

(a) (b)

Fig. 14. (a) Flash formation on the CR, (b) deposit on the substrate

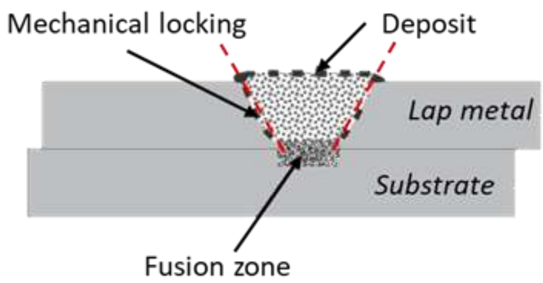

Fig. 15. Schematic of the spot lap joint. The red dashed line indicates the slanted side of the V-groove holes.

Fig. 14(a) illustrates the rod following friction surfacing (FS), showing plastic deformation at the rod tip or flash. This occurs because of axial force/pressure and the consumable rod (CR) during FS. Flash formation on consumable substrate (CS) is associated with lateral expansion of the deposit dimension. This widening, resulting from viscoplastic deformation flow at the CS tip (Fig. 14(b)), can be leveraged for metal lap joining. The expanded dimension covers the beveled edge of the lap joint hole, providing mechanical locking (Fig. 15) and enhancing lap-joint strength in addition to the fusion zone. The formed layer thickness can cover the depth of lap joint hole. A limitation is that the layer/deposit width may be smaller than the diameter of the CR (Table II), causing gaps or voids in the layer/deposit or at the interface and reducing joint strength. However, because deposit dimension is influenced by axial pressure, this issue can be addressed by increasing FS axial load/pressure. The lap-joint groove scheme is shown in Fig. 16.

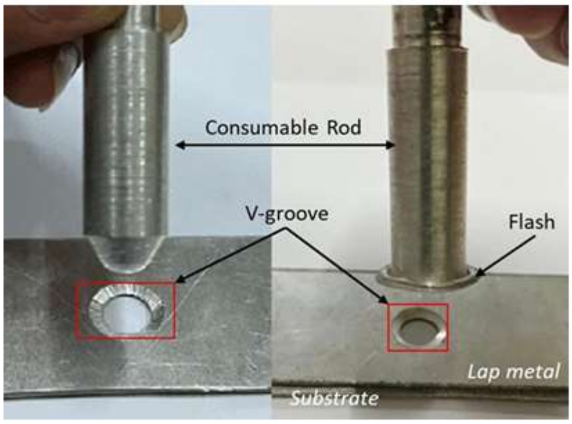

Fig. 16. Consumable rod before friction surfacing and consumable rod after friction surfacing with flash

The mechanical strength of lap joints is affected by axial force application and substrate surface roughness. As shown in Fig. 14 and 15, axial forces significantly increased bending strength and hardness between the substrate and deposit. Conversely, substrate surface roughness reduced bending strength, but it remained higher than that of the parent material (AA1100) or was optimized to less than 2.21 µm.

Thus, FS without travel speed or Spot Friction, combined with the concept of joint parameters used in conventional welding processes, could be adapted and applied for lap joining techniques to improve joint quality, consistency, and durability and to expand this process's applications in manufacturing industries requiring high-strength reliable aluminum joints

IV. CONCLUSIONS

The characteristics of friction-surfaced deposits, including dimensions, bending strength, and hardness, are significantly affected by axial force/pressure, consumable rod diameter, and surface roughness. This study demonstrates that Spot Friction parameters, including rotational speed, CS dimensions, and axial load, combined with metal joining parameters such as joint angle and substrate surface roughness, can develop a novel aluminum joining technique. Further investigation is warranted.

ACKNOWLEDGMENT

Gratitude is expressed to the program of BIMA Diktisaintek (PTM) of Indonesia. The authors also acknowledge The Centre of Research and Development for Metallurgy Universitas Hasanuddin for facilitating access to the laboratories and library and for valuable academic discussions.

REFERENCES

[1] A. Kar, A. Sharma, and S. Kumar, "A Critical Review on Recent Advancements in Aluminium-Based Metal Matrix Composites," *Crystals (Basel).*, vol. 14, no. 5, 2024,

[2] A. A. Alghannam *et al.*, "Investigation on mechanical properties and corrosion resistance of Ti-modified AA5083 aluminum alloy for aerospace and automotive applications," *Sci. Rep.*, vol. 13, no. 1, pp. 1–10, 2023,

[3] D. Istrate *et al.*, "Correlation between Mechanical Properties—Structural Characteristics and Cavitation Resistance of Rolled Aluminum Alloy Type 5083," *Metals (Basel).*, vol. 13, no. 6, 2023,

[4] S. Nagaraja *et al.*, "Friction stir welding of dissimilar Al-Mg alloys for aerospace applications: Prospects and future potential," *Reviews on Advanced Materials Science*, vol. 63, no. 1, Jan. 2024, doi: 10.1515/rams-2024-0033.

[5] N. Muhayat *et al.*, "Apparatus Design of One-Step Double-Side Friction Stir Welding for Aluminum Plates," *Designs (Basel).*, vol. 7, no. 3, Jun. 2023

[6] E. Hoyos and M. C. Serna, "Basic tool design guidelines for friction stir welding of aluminum alloys," *Metals (Basel).*, vol. 11, no. 12, Dec. 2021.

[7] M. M. El-Sayed Seleman *et al.*, "The Additive Manufacturing of Aluminum Matrix Nano Al2O3 Composites Produced via Friction Stir Deposition Using Different Initial Material Conditions," *Materials*, vol. 15, no. 8, Apr. 2022

[8] M. M. Z. Ahmed, M. M. El-Sayed Seleman, E. Elfishawy, B. Alzahrani, K. Touileb, and M. I. A. Habba, "The effect of temper condition and feeding speed on the additive manufacturing of AA2011 parts using friction stir deposition," *Materials*, vol. 14, no. 21, Nov. 2021.

[9] M. Newishy, M. Jaskari, A. Järvenpää, H. Fujii, and H. A. Abdel-Aleem, "Friction Stir Welding of Dissimilar Al 6061-T6 to AISI 316 Stainless Steel: Microstructure and Mechanical Properties," *Materials*, vol. 16, no. 11, Jun. 2023.

[10] M. Hoffmann, E. A. Duda, P. Aspes, and B. Klusemann, "Effect of ambient conditions in friction surfacing," *Welding in the World*, vol. 69, no. 2, pp. 397–406, Feb. 2025.

[11] S. Sundaram and M. Kumarasamy, "Joint characteristics and process parameters optimization on friction stir welding of AA 2024-T6 and AA 5083-H111 aluminum alloys," *Journal of the Serbian Chemical Society*, vol. 89, no. 10, pp. 1387–1399, 2024.

[12] R. Bharathikanna and G. Elatharasan, "Microstructure, Mechanical and Corrosion Behavior of Friction Stir Processed AA6082 with Cr3C2 Particles," *Soldagem e Inspecao*, vol. 27, 2022.

[13] Z. Kallien, M. Hoffmann, A. Roos, and B. Klusemann, "Correlation of Microstructure and Local Mechanical Properties Along Build Direction for Multi-layer Friction Surfacing of Aluminum Alloys," *JOM*, vol. 75, no. 10, pp. 4212–4222, Oct. 2023, doi: 10.1007/s11837-023-06046-4.

[14] Z. Kallien *et al.*, "Combining fusion-based and solid-state additive manufacturing: Investigation of additive DED structures with friction surfacing interlayer," *Additive Manufacturing Letters*, vol. 14, Jul. 2025.

[15] P. Samal, H. Raj, A. Meher, B. Surekha, P. R. Vundavilli, and P. Sharma, "Synergistic Effect of B4C and Multi-Walled CNT on Enhancing the Tribological Performance of Aluminum A383 Hybrid Composites," *Lubricants*, vol. 12, no. 6, Jun. 2024.

[16] M. Mortello, M. Pedemonte, N. Contuzzi, and G. Casalino, "Experimental investigation of material properties in FSW dissimilar aluminum-steel lap joints," *Metals (Basel).*, vol. 11, no. 9, Sep. 2021.

[17] M. Regev and S. Spigarelli, "On Dynamic Recrystallization during the Friction Stir Processing of Commercially Pure Ti and Its Influence on the Microstructure and Mechanical Properties," *Metals (Basel).*, vol. 14, no. 6, Jun. 2024.

[18] H. H. Kinfu and M. M. Rahman, "Separation Performance of Membranes Containing Ultrathin Surface Coating of Metal-Polyphenol Network," May 01, 2023, *MDPI.*

[19] U. M. Jamaludeen, "Examination and Optimization of Friction Stir Welding Process Parameters of AA6092 Alloys," *Soldagem e Inspecao*, vol. 29, 2024.

[20] M. A. R. Pereira, I. Galvão, J. D. Costa, A. M. Amaro, and R. M. Leal, "Joining of Fibre-Reinforced Thermoplastic Polymer Composites by Friction Stir Welding—A Review," Mar. 01, 2022, *MDPI*.

[21] S. Saravanakumar *et al.*, "Optimizing friction stir processing parameters for aluminium alloy 2024 reinforced with SiC particles: A taguchi approach of investigation," *Journal of Materials Research and Technology*, vol. 30, pp. 4847–4855, May 2024.

[22] D. O. Bokov *et al.*, "Effect of pin shape on thermal history of aluminum-steel friction stir welded joint:

Computational fluid dynamic modeling and validation," *Materials*, vol. 14, no. 24, Dec. 2021.

[23] P. Kahhal, M. Ghasemi, M. Kashfi, H. Ghorbani-Menghari, and J. H. Kim, "A multi-objective optimization using response surface model coupled with particle swarm algorithm on FSW process parameters," *Sci. Rep.*, vol. 12, no. 1, Dec. 2022.

[24] B. Ahmad, F. Almaskari, J. Sheikh-Ahmad, S. Deveci, and K. Khan, "Thermomechanical Modeling of Material Flow and Weld Quality in the Friction Stir Welding of High-Density Polyethylene," *Polymers (Basel).*, vol. 15, no. 15, Aug. 2023.

[25] A. I. Alhatti, J. Sheikh-Ahmad, F. Almaskari, K. A. Khan, S. Deveci, and A. I. Hosny, "A Study of the Friction Stir Lap Welding of AA5052 and Polypropylene," *Polymers (Basel).*, vol. 15, no. 23, Dec. 2023.

[26] M. I. A. Habba *et al.*, "Comparative Study of FSW, MIG, and TIG Welding of AA5083-H111 Based on the Evaluation of Welded Joints and Economic Aspect," *Materials*, vol. 16, no. 14, Jul. 2023.

[27] W. Song *et al.*, "Effects of Friction Stir Processing on the Microstructure and Mechanical Properties of an Ultralight Mg-Li Alloy," *Crystals (Basel).*, vol. 14, no. 1, Jan. 2024.

[28] S. Barella, M. Belfi, A. Gruttadauria, C. Liu, and Y. Peng, "Metallurgical and Mechanical Investigation on Single-Step Quenching and Partitioning Thermal Treatments on Commercial Low Alloyed 30MnV6 Steel," *Metall. Mater. Trans. A Phys. Metall. Mater. Sci.*, vol. 55, no. 2, pp. 513–522, Feb. 2024.

[29] V. Palanivel, P. Johnson, A. Munimathan, and S. T. Arumugam, "Finite element analysis of friction stir welding process to predict temperature distribution," *Revista Materia*, vol. 29, no. 4, 2024.

[30] A. Debih and H. Azzeddine, "Influence of tool rotational speed on the microstructure and mechanical behavior of friction stir processed AA 7050 aluminum alloy," *Kovove Materialy*, vol. 62, no. 2, pp. 91–100, 2024.

[31] X. Zhu, R. Wang, L. Wang, M. Liu, and S. Li, "Effect of Rotational Shear and Heat Input on the Microstructure and Mechanical Properties of Large-Diameter 6061 Aluminium Alloy Additive Friction Stir Deposition," *Crystals (Basel).*, vol. 14, no. 7, Jul. 2024.

[32] C. Kahra *et al.*, "Intermetallic Compound Layer Morphology and Distribution in Friction-Welded Steel–Aluminum Components," *Adv. Eng. Mater.*, vol. 27, no. 16, Aug. 2025.

[33] M. Hossfeld, "On Friction, Heat Input, and Material Flow Initiation during Friction Stir Welding: Tool and Process Optimization," *Journal of Manufacturing and Materials Processing*, vol. 7, no. 1, p. 34, Jan. 2023.

[34] X. Xiao, Y. Mao, X. Wang, D. Qin, and L. Fu, "Effects of Curvature Direction on Friction Stir Welding Lap Joint of Aluminum Alloy 'S' Curved Surface," Jan. 11, 2023.

[35] G. Cao, J. Wang, B. Gao, K. Mu, H. Zhang, and B. Li, "a new type of plug-in friction-stir lap welding based on the 6061-t6 aluminum alloy," *Materiali in Tehnologije*, vol. 58, no. 1, pp. 103–110, 2024.

[36] D. K. Sahoo, A. N. Chari, and A. S. Reddy, "Optimization & characterization of friction surfaced coatings of AA6063 aluminium alloy over AISI316 stainless steel substrate," in *Materials Today: Proceedings*, Elsevier Ltd, 2020, pp. 565–572.

[37] L. O. P. da Silva, T. N. Lima, F. M. dos S. Júnior, B. Callegari, L. F. Folle, and R. S. Coelho, "Heat-Affected Zone Microstructural Study via Coupled Numerical/Physical Simulation in Welded Superduplex Stainless Steels," *Crystals (Basel).*, vol. 14, no. 3, Mar. 2024.

[38] W. Zhang, H. Gao, D. Liu, Y. Gao, Y. Zhang, and L. Kong, "Effects of Heat Treatment on Microstructures and Mechanical Properties of a Low-Alloy Cylinder Liner," *Materials*, vol. 17, no. 4, Feb. 2024.

[39] N. A. Alsaleh *et al.*, "Additively Manufactured Parts from AA2011-T6 Large-Diameter Feedstocks Using Friction Stir Deposition," *Materials*, vol. 16, no. 14, Jul. 2023.

[40] S. Gao, C. Wu, X. Yang, J. Cheng, and R. Kang, "Study on Adhesion Properties and Process Parameters of Electroless Deposited Ni-P Alloy for PEEK and Its Modified Materials," *Coatings*, vol. 13, no. 2, Feb. 2023.

[41] E. Altuncu and M. Tarım, "investigation of the bending behavior of inc625/sus316l laser-cladding layers applied to ggg40," *Materiali in Tehnologije*, vol. 58, no. 3, pp. 363–370, 2024.

[42] G. Chudasama, S. Wanare, and V. Kalyankar, "influence of substrate surface roughness on push-off strength for friction surfacing of low carbon steel with aa6061-t6 aluminium alloy," *International Journal of Modern Manufacturing Technologies*, vol. 15, no. 2, pp. 56–62, 2023.

[43] M. Movahedi, M. Mohsenirad, and A. Ozlati, "Aluminum surface treatment and process optimization: Boosting mechanical performance in aluminum/polypropylene composite friction stir lap joints," *Journal of Advanced Joining Processes*, vol. 11, Jun. 2025.

[44] A. Vyas and A. Aliyu, "Structural and mechanical properties of Si-doped CrN coatings deposited by magnetron sputtering technique," *Heliyon*, vol. 9, no. 2, Feb. 2023, doi: 10.1016/j.heliyon.2023.e13461.

[45] P. Ellakany, M. Madi, N. M. Aly, T. Alshehri, S. T. Alameer, and F. A. Al-Harbi, "Influences of Different CAD/CAM Ceramic Compositions and Thicknesses on the Mechanical Properties of Ceramic Restorations: An In Vitro Study," *Materials*, vol. 16, no. 2, Jan. 2023.